Desalination and Water Treatment
www.deswater.com
doi: 10.1080/19443994.2015.1051126

57 (2016) 12632–12643
June

Taylor & Francis
Taylor & Francis Group

Copper ions removal from aqueous solutions by novel Ca–Al–Zn layered double hydroxides

A.A. Bakr[a,*], Gh. Eshaq[b], A.M. Rabie[b], A.H. Mady[b], A.E. ElMetwally[b]

[a]*Department of Analysis and Evaluation, Egyptian Petroleum Research Institute (EPRI), Nasr City, Cairo 11727, Egypt, Tel. +20 1227135228; email: als_water@yahoo.com*
[b]*Department of Petrochemicals, Egyptian Petroleum Research Institute (EPRI), Nasr City, Cairo, 11727, Egypt, Tel. +20 1003056808; email: ghadaamer2002@yahoo.com (Gh. Eshaq), Tel. +20 1228289661; email: abdo3040@yahoo.com (A.M. Rabie), Tel. +20 1112724232; email: amr_mady@yahoo.com (A.H. Mady), Tel. +20 1115025588; email: ahmed_ezzatt@msn.com (A.E. ElMetwally)*

Received 24 November 2014; Accepted 5 May 2015

ABSTRACT

Novel Ca–Al–Zn layered double hydroxide (LDH) was synthesized by co-precipitation method and its calcined product (calcined Ca–Al–Zn LDH) was obtained by heating at 450°C for 4.0 h. The calcined and uncalcined products of Ca–Al–Zn LDHs were used as adsorbents to remove copper ions from aqueous solutions. The structure, composition, and morphology of the synthesized calcined and uncalcined products were approved by X-ray diffraction, FT-IR, N_2 adsorption–desorption isotherm, and scanning electron microscopy. The removal capacities of calcined layered double hydroxide are higher than that of uncalcined LDH at ambient temperature, different pH, constant shaking rate 160 rpm, and different copper/adsorbent ratios. According to the analytical results and the experimental data, we were successful to prepare a novel LDH adsorbent for the Cu(II) removal, where the removal of the copper ions reached a maximum value at pH 6.0, shaking, 160 rpm, adsorbent mass 0.25 g/l and after 120 min to be 15.4 and 20.5 mg of Cu(II) per gram of uncalcined and calcined LDH, respectively. According to these results, the calcined Ca–Al–Zn LDH has higher potential application in Cu(II) ions removal field.

Keywords: Water treatment; Ca–Al–Zn LDH; Cu(II) removal; Calcination

1. Introduction

The LDHs having the general formula $[M^{2+}_{(1-X)}M^{3+}_{X}(OH)_2]^{X+}[A_{n-x/n}mH_2O]^{x-}$, M^{2+} = divalent cations; M^{3+} = trivalent cations, A is the interlayer anion and *n* represents the number of water molecules. The creation of such positive charge is the key factor in LDH to intercalate and exchange different organic and inorganic anions. These materials consist of positively charged metal hydroxide sheets composed of edge-shared octahedral network. The positive charge on the metal hydroxide sheets are neutralized by exchangeable charge balancing anions present in the interlamellar space besides water molecules. The calcination of LDH containing carbonate as interlayer anion causes the formation of $M^{2+}M^{3+}O$ solid solution capable of recovering the LDH layered structure upon treatment with water or aqueous solution containing various anions via the so-called memory effect [1–4]. The

*Corresponding author.

calcination temperature must be high enough to eliminate most of the anions of the interlayer. However, if the calcination temperature is too high such as higher than 600˚C, stable $M^{3+}M_2^{2+}O_4$ spinel and $M^{2+}O$ phases are formed and LDHs cannot be reconstructed. By heating LDHs above 400˚C, the interlayer CO_3^{2-} can be removed and the resulting calcined LDH can be used for removing inorganics by either adsorption on the external surface of the layers, intercalation process, or reconstruction behavior [5–9].

For these layered compounds, the most studied are the aluminum-based ones such as Mg/Al and Zn/Al hydrotalcites and their calcined products [10]. Therefore, in order to reduce Al content, as well as try not to affect the adsorption capacity as much as possible, Al was substituted partly for another metal ion. So, Mg–Al–Fe hydrotalcite compound was synthesized and modificated by calcinations (HTlc 500) [11,12]. Various treatment methods such as chemical precipitation, reverse osmosis, ion exchange, solvent extraction, coagulation, and adsorption are utilized to remove metal ions from aqueous solutions. However, due to the economic constraints which the country is facing, a development of cost-effective and clean processes is desired. Of all these methods, adsorption has proved to be the most effective, especially for effluents with moderate and low concentrations [13,14].

The efficiency of adsorption depends on many factors, including the surface area, pore size distribution, polarity, and functional groups of the adsorbent [15]. The kinetics and thermodynamics of ferrous removal by novel Co/Mo LDH from aqueous solutions [16] and some LDHs containing varying amounts of Al^{3+}, Zr^{4+}, and Zn^{2+} or Mg^{2+} in the metal hydroxide layer have been used in Cr(VI) and Se(IV) adsorption [17]. While the optimum copper concentration in drinking water for general good health set by World Health Organization (WHO) guideline value is less than 2.0 mg/l [18], the uptake of Cu(II) ions from aqueous solutions was carried out by different materials such as magnetic nano-composite beads [19]. While, in another literature, micro-size magnetic polymer adsorbent coupling with metal-chelating ligands of iminodiacetic acid was found to be able to load 7.68 mg/g of copper ions [20]. Also, the results showed that the maximum uptakes of Cu^{2+} on LDH-H100, LDH-H50, and LDH-Cl were 0.76, 1.02, and 1.95 mmol/g, respectively [21].

The objectives of this study were (a) synthesize a novel Ca–Al–Zn LDH; (b) characterize the structure of the synthesized Ca–Al–Zn LDH and its calcined product by XRD, FT-IR, N2 adsorption–desorption isotherm, and scanning electron microscopy (SEM); and (c) determine the influence of different parameters viz. solution pH, calcined temperature, adsorbent mass, contact time, and initial copper ions concentrations on their performance in the adsorption of copper from aqueous solutions.

2. Materials and methods

2.1. Materials

All chemicals with a purity of greater than 99.9% were purchased as follows: copper nitrate pentahemihydrate ($Cu(NO3)_2{\cdot}2½H_2O$) was purchased from Sigma-Aldrich Co.; $Al(NO_3)3{\cdot}9H_2O$, K_2CO_3, and KOH were obtained from Sigma-Aldrich and $Ca(NO_3)_2{\cdot}4H_2O$; and $Zn(NO_3)_2{\cdot}6H_2O$ were purchased from Loba Chemie Co.

2.2. Synthesis of Ca–Al–Zn LDH

The LDHs containing Ca–Al–Zn were prepared by co-precipitation method at low supersaturation conditions and at constant pH [22]. An aqueous solution (A, 1.0 M) was prepared, containing the dissolved salts of $Ca(NO_3)_2{\cdot}4H_2O$, $Zn(NO_3)_2{\cdot}6H_2O$, and $Al(NO_3)_3{\cdot}9H_2O$ in the required amounts. Meanwhile, an alkaline solution (B, 2.0 M) was prepared, containing K_2CO_3 and KOH. Solutions (A) and (B) were added simultaneously to a glass reactor, containing previously 100 cm^3 of deionized H_2O, at a controlled pH of 9. The precipitate obtained was kept under vigorous mechanical stirring, at a temperature of 80˚C for 18 h. Afterward, the product was thoroughly washed with hot deionized water in order to eliminate excess ions and dried at 100˚C for 24 h. The M^{II}/M^{III} molar ratio was kept constant at 2.

The obtained samples were calcined at 450˚C for 5 h prior to adsorption. For instance, to prepare 100 g of a Ca–Al–Zn LDH with 15% wt. of zinc, the following amounts were used: $Ca(NO_3)_2{\cdot}4H_2O$ = 168.07 g, $Zn(NO_3)2{\cdot}6H_2O$ = 68.13 g, and $Al(NO_3)_3{\cdot}9H_2O$ = 117.7 g, dissolved in 1,097.7 ml of distilled water [23].

2.3. Characterization of Ca–Al–Zn LDH

2.3.1. X-ray diffraction (XRD)

XRD patterns of the samples were recorded in the range 2θ = 4–80˚ using a Philips powder diffractometer with Cu Kα radiation (k = 0.154 nm). The instrument was operated at 40 kV and 40 mA. The spectra were recorded with a 2θ step of 0.02˚ at a scanning rate of $2^{\circ}\theta$/min.

2.3.2. Infrared spectroscopy

Fourier transform infrared spectroscopy (FTIR) measurements were performed using a Nicolet IS-10 FTIR instrument with KBr disks.

2.3.3. Scanning electron microscopy

SEM images of the gold-coated catalysts were obtained using a JEOL 5410 system operating at 20 kV.

2.3.4. Textural analysis

Surface area, pore volume, and average pore size were obtained from the N_2 adsorption–desorption isotherms determined at −196°C using a Quantachrome Nova 3200 instrument (USA). Prior to measurements, the samples were perfectly degassed at 100ºC for 12 h under vacuum (10–5 mmHg).

2.4. Adsorption experiments

The copper ions, Cu(II), stock solution concentration of 100 mg/l was prepared by dissolving copper nitrate pentahemihydrate ($Cu(NO_3)_2{\cdot}2½H_2O$) in distilled water. The working Cu(II) solution concentration ranging from 10 to 55 mg/l for all experiments was freshly prepared from the stock solution. Standard acid (0.01 M HNO_3) and alkaline solutions (0.125 M NaOH) were used for pH adjustments at pH 2, 3, 4, 5, 6, 7, 8, 9, and 10. The pH of the solution was measured with a pH meter (Mettler-Toledo AG 8603 Schwerzenbach, made by Mettler-Toledo Group). The pH meter was calibrated with buffers of pH 4.0–7.0 before any measurement.

The removal of Cu(II) from dilute aqueous solutions, addition of adsorbent (calcined and uncalcined Ca–Al–Zn LDH) masses 0.10, 0.15, 0.20, 0.25, 0.30, 0.35, 0.40, 0.45, 0.50, and 0.55 g/l were carried out at constant temperature 25°C, using distilled water. After continuous stirring, over a magnetic stirrer at 160 rpm for a predetermined time interval 10, 20, 30, 60, 90, 120, 150, and 180 min to allow the dispersion of adsorbent and metal ions to reach equilibrium conditions, as found during preliminary experiments. The solid and solution were separated by centrifugation at 3,000 rpm for 15 min and slightly dried at ambient temperature. Cu(II) concentration was determined by Spectrophotometer, LaMotte, model SMART Spectro, USA, and the solid phase was analyzed. The amount of adsorption q_e (mg/g) and the percentage of removal (% removal) were calculated by the following equations [24]:

$$q_e = (C_0 - C_e) \times V/m \quad (1)$$

$$\%\,\text{Removal} = (C_0 - C_e)/C_0 \times 100\% \quad (2)$$

where C_0 and C_e are the initial Cu(II) concentration and the concentration at equilibrium in mg/l, m is the mass of the adsorbent, and V is the volume of solution.

2.5. Effect of initial solution pH

The effect of initial solution pH on copper ions removal was evaluated by making a series of 55 mg/l Cu(II) solutions at an adsorbent dosage of 0.25 g/l, the starting solution pH was adjusted to the designed values (2, 3, 4, 5, 6, 7, 8, 9, and 10). The resulting calcined and uncalcined Ca–Al–Zn LDHs suspensions were filtered, and then, the residual Cu(II) concentrations were analyzed.

2.6. Effect of adsorbent mass

Different amounts of Ca–Al–Zn LDHs (0.10, 0.15, 0.20, 0.25, 0.30, 0.35, 0.40, 0.45, 0.50, and 0.55 g/l) were added to a series of 100 ml of copper solutions with initial concentration of 55 mg/l at pH 6.0, and shaken rate 160 rpm for different contact time (10, 20, 30, 60, 90, 120, 150, and 180 min) to reach the equilibrium. Then, the aqueous samples were filtered, and then, the residual Cu(II) concentrations were analyzed.

3. Results and discussion

3.1. Characterization of Ca–Al–Zn LDH

3.1.1. X-ray diffraction

The XRD patterns of Ca–Al–Zn LDH catalysts before and after copper adsorption are shown in Fig. 1 and the XRD patterns of the calcined Ca–Al–Zn LDH catalysts before and after copper adsorption are shown in Fig. 2. The XRD pattern of Ca–Al–Zn LDH is shown in Fig. 1(a). It is found that more intense peaks are located at lower 2θ while less intense lines are present at higher 2θ values. It is obvious that the XRD pattern of Ca–Al–Zn LDH in Fig. 1(a) exhibits the Bragg reflections of basal planes. The sharp and symmetric peaks at the basal (0 0 3), (0 0 6), and (1 1 0) reflections around $2\theta \sim 11^\circ$, $2\theta \sim 23^\circ$, and $2\theta \sim 60^\circ$, respectively, correspond to the basal and in-plane spacing, with a high degree of crystallinity. In addition, the d003 spacing was found to be 7.8 Å, which is within

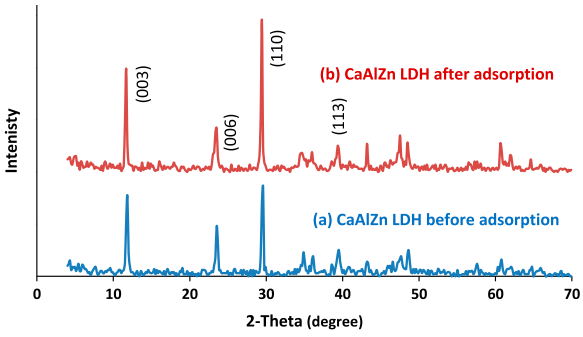

Fig. 1. XRD patterns of the prepared Ca–Al–Zn LDH: (a) before and (b) after Cu(II) adsorption.

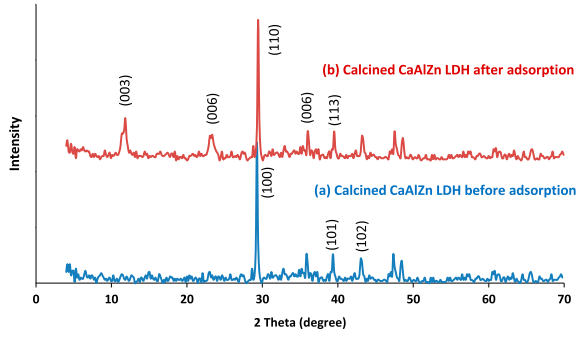

Fig. 2. XRD patterns of the calcined Ca–Al–Zn LDH: (a) before and (b) after Cu(II) adsorption.

the accepted range for a LDH structure. Fig. 1(b) shows the pattern of Ca–Al–Zn LDH after copper adsorption, the features at (0 0 3), (0 0 6), and (1 1 0) are essentially retained after copper adsorption, which indicates that the adsorption of copper on Ca–Al–Zn LDH takes place via surface adsorption. The XRD pattern of the calcined Ca–Al–Zn LDH (Fig. 2(a)) shows that the structure of the Ca–Al–Zn LDH is decomposed upon calcination at 450°C for 5 h. After calcination, the (0 0 3) and (0 0 6) reflections practically disappear, indicating that the Ca–Al–Zn LDH structure is destroyed and the stacking of the layers becomes disordered. Only few diffused peaks at 32° and 73° are observed, which are attributed to ZnO. Fig. 2(b) shows the diffraction pattern of the calcined Ca–Al–Zn LDH after copper adsorption. The reappearance of the characteristic layered structure of Ca–Al–Zn LDH at (0 0 3), (0 0 6), and (1 1 0) is an indication for the "memory effect" of the Ca–Al–Zn LDH. Unit cell parameters *c* and *a*, listed in Table 1, are obtained by Bragg's law. The unit cell parameter a is related to the cation–cation distance within the layer, and its value depends on the nature of the cations [25]. The unit cell parameter *c* is related to the thickness of the layer and the interlayer distance according to hexagonal stacking. Table 1 represents the crystal sizes, which are calculated using Scherrer's equation.

3.1.2. FTIR analysis

The Fourier transform infrared spectra of the prepared Ca–Al–Zn LDH before and after copper adsorption are shown in Fig. 3, while that of the calcined Ca–Al–Zn LDH before and after copper adsorption are shown in Fig. 4. As shown in Figs. 3 and 4, the broad absorption at 3,444–3,500 cm^{-1} is assigned to the O-H stretching vibration of the water molecule [26–31]. The peak at 1,640 cm^{-1} is assigned to the bending mode of O–H in water molecule [32]. The weak shoulder peak occurs at about 3,000 cm^{-1} is assigned to the OH stretching mode of interlayer water molecules hydrogen-bonded to interlayer anions. A characteristic band in the low-frequency region is corresponding to vibration modes and ascribed to M–O vibration at 1,000 cm^{-1} [33]. In addition, a strong band at 1,370 cm^{-1} indicates the presence of CO_3^{2-} anions in the interlayer region [32]. The weak shoulder at 788 cm^{-1} can be attributed to Al–O bond vibrations.

3.1.3. Morphological structure

The SEM images of the prepared Ca–Al–Zn LDH before and after copper adsorption are shown in Fig. 5(a) and (b), while that of the calcined Ca–Al–Zn LDH before and after copper adsorption are shown in Fig. 5(c) and (d). It is obvious that the structure of the LDH presented in Fig. 5(a) and (b) shows an aggregated mass of irregularly shaped tiny particles with a highly porous structure. However, after calcination, the adsorbent irregular particles became well dispersed and the particle size is distributed as shown in Fig. 5(c) and (d). The small particle size and the porous structure provide a good adsorption capacity for copper. Fig. 5(b) and (d) shows that the surface of Ca–Al–Zn LDH and the calcined Ca–Al–Zn LDH after copper adsorption exhibits a reconstructed surface with a plate-like morphology that is completely different from that of the clean surface before copper adsorption. Compared with the morphology of platelets, the full extent of adsorption of copper onto Ca–Al–Zn LDH and calcined Ca–Al–Zn LDH cannot be observed, which may be due to the high level of crystallinity of this adsorbent.

Table 1
Unit cell parameters and crystal sizes

Sample	Unit cell parameters (Å)		Interlayer distance (Å)[a]	Crystal size (Å)[b]	
	c	*a*		L_{003}	L_{110}
Ca–Al–Zn LDH	17.06	4.98	7.8	49.2	76

[a]Calculated considering the thickness of the hydrotalcites as 7.8 Å.
[b]Calculated using Scherrer's equation.

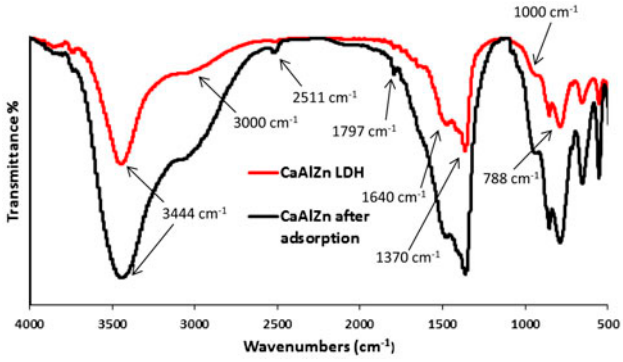

Fig. 3. FTIR spectra of the prepared Ca–Al–Zn LDH (before and after adsorption).

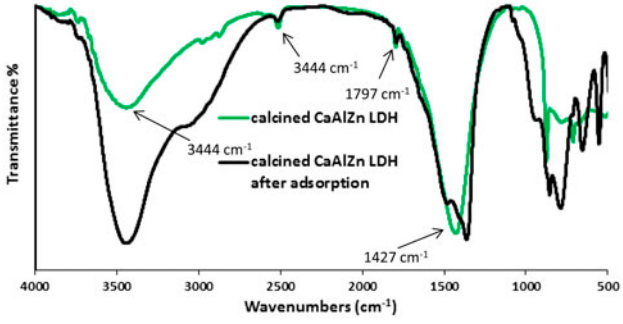

Fig. 4. FTIR spectra of the calcined Ca–Al–Zn LDH (before and after adsorption).

3.1.4. Chemical and textural analyses

Elemental analysis of Ca–Al–Zn LDH was performed using X-ray fluorescence (XRF) instrument with channel control model Pw1390 (Philips) and spectrometer model Pw 1410. The real M^{II}/M^{III} molar ratio of Ca–Al–Zn LDH with a chemical composition of $Ca_{0.49}$ $Al_{0.33}$ $Zn_{0.18}$ $(CO_3)_{0.18}{\cdot}H_2O$ was found to be 2.03, where the M^{II}/M^{III} nominal molar ratio was kept constant at 2 during the synthesis. As M^{II}/M^{III} increases, the number of structural charges decreases, producing a lower exchange capacity of the adsorbent [23].

The adsorption–desorption isotherm of the prepared Ca–Al–Zn LDH is shown in Fig. 6 and that of the calcined Ca–Al–Zn LDH is shown in Fig. 7. They can be classified as type IV according to IUPAC classification exhibiting H3 hysteresis loop [34]. This type indicates the presence of aggregates (assemblage of particles which are loosely coherent) of plate-like particles giving rise to slit-shaped pores with nonuniform size and shape [35]. The isotherms display hysteresis loops closes at $(P/P_o) < 0.2$. The value of average pore radius r that represents half the slit width is calculated as $r = (Vp/A_{BET})$, where Vp is the total pore volume taken at $P/P_o \approx 1.0$, and A_{BET} is the specific surface area obtained using the BET equation, taken at $P/P_o = 0.98$ [34,36]. The values listed in Table 2 indicate that the full width of pores of the prepared Ca–Al–Zn LDH and calcined Ca–Al–Zn LDH is 48.6 and 88.7 Å, respectively, which lies within the initial part of the range of pore sizes that assigned to mesoporosity. The pore size distribution values were determined by the Brunauer–Joyner–Hallenda (BJH) method applied to the desorption branch, and *t*-plot method was used to calculate the type of pores [37]. Thus, the calcined Ca–Al–Zn LDH has higher value of A_{BET}, higher value of Vp, and average pore radius than that of the prepared Ca–Al–Zn LDH. Therefore, the higher extent of the adsorption of copper in case of the calcined Ca–Al–Zn LDH can be attributed to the higher surface area, presence of a relatively greater number of narrow mesopores and total pore volume that are known to furnish a high measurable adsorption capacity than the prepared Ca–Al–Zn LDH. This could be explained as the calcination of Ca–Al–Zn LDH may result in an increase in the interlayer spaces distortion resulting in an increase in the area and increase in the total pore volume and pore radius.

The pore size distribution curves were obtained using BJH calculation method [38], for desorption branch data as shown in Figs. 8 and 9. The curve of Ca–Al–Zn confirms the presence of two sizes of pores, a peak at 20 Å, and a broader one centered at 46 Å.

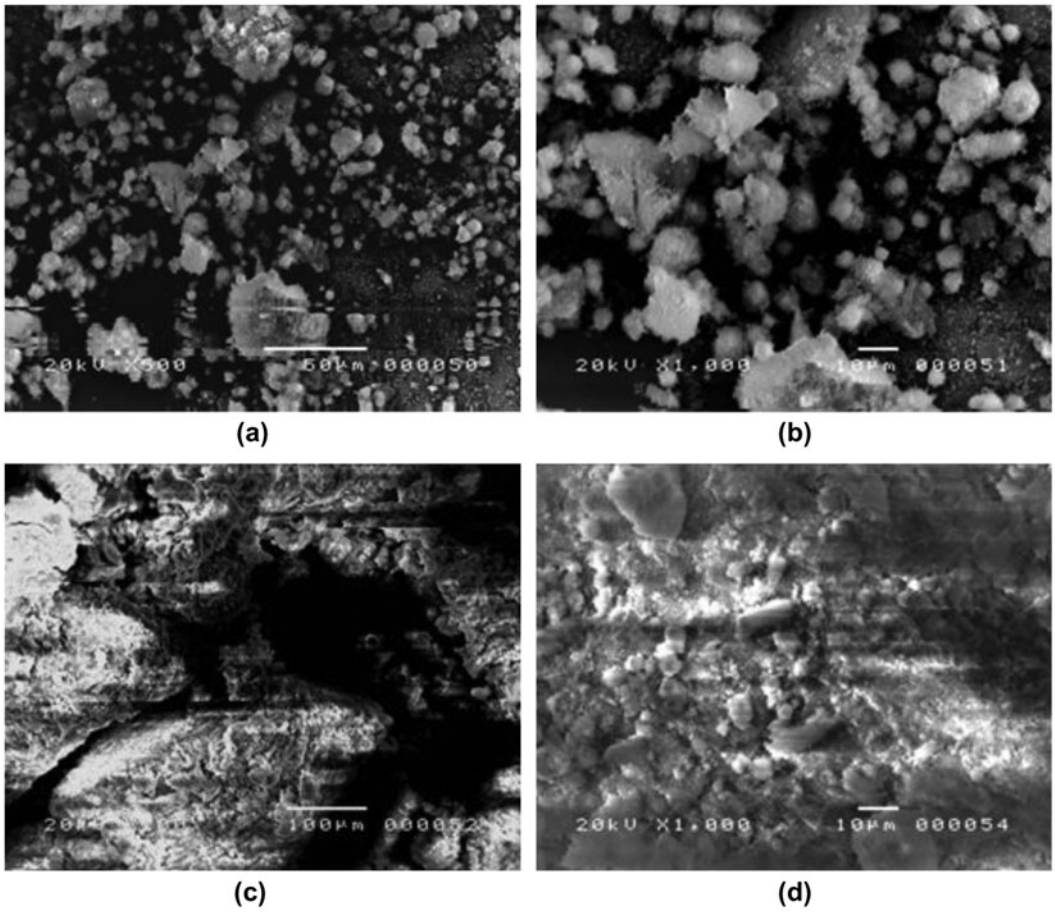

Fig. 5. SEM images of the prepared Ca–Al–Zn LDH: (a) before and (b) after adsorption, and the images of the calcined Ca–Al–Zn LDH: (c) before and (d) after adsorption.

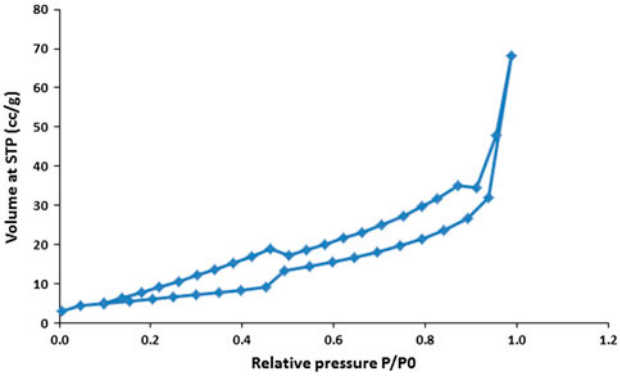

Fig. 6. N_2 adsorption–desorption isotherm of the prepared Ca–Al–Zn LDH.

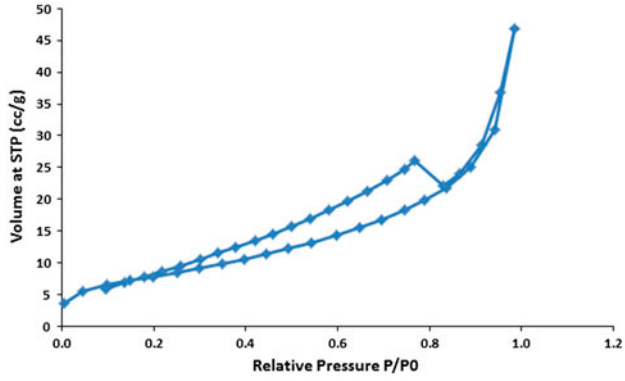

Fig. 7. N_2 adsorption–desorption isotherm of the calcined Ca–Al–Zn LDH.

Also, the shape of deviation implies the presence of two sizes of mesopores; on the other hand, it agrees with the width of the hysteresis loop. This can be interpreted as before calcination the microstructure of the LDH can be clearly observed as aggregated mass of irregularly shaped tiny particles [39]. The calcined

Table 2
Surface data of the prepared Ca–Al–Zn LDH and calcined Ca–Al–Zn LDHs

Sample	A_{BET} (m^2/g)	V_p (ml/g)	$r = V_p/A_{BET}$ (Å)	*C*-value in BET equation
Ca–Al–Zn LDH	22.5	0.07	24.4	76.105
Calcined Ca–Al–Zn LDH	28.7	0.1	44.44	84.96

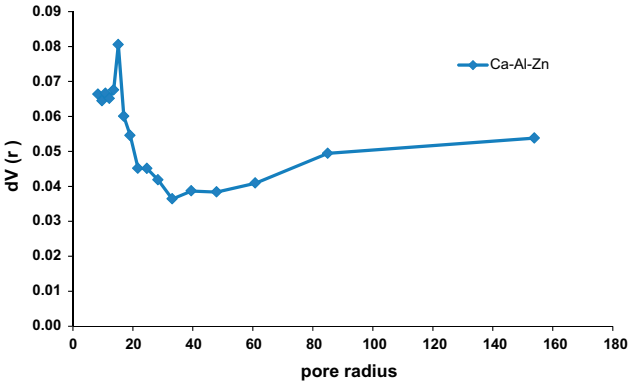

Fig. 8. Pore size distribution for Ca–Al–Zn LDH.

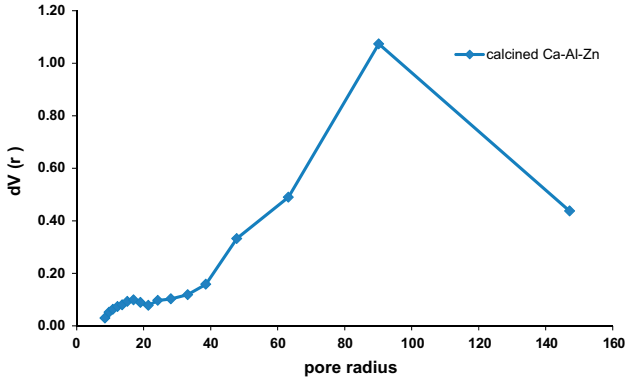

Fig. 9. Pore size distribution for calcined Ca–Al–Zn LDH.

Ca–Al–Zn curve displays a defined peak appeared from 45 Å with a maxima centered at 90 Å, which supports the belief that there is a relatively greater number of narrow mesopores and macropores stemmed from both the shape of adsorption isotherm and width of the prevailing hysteresis loop in the adsorption isotherm. After calcination, the adsorbent becomes into irregular particles which disperse well and the particle size distributes from a few nano to microns [39]. The small particle size and the porous structure provide a good adsorption capacity for Cu(II).

3.2. Effect of initial Cu(II) concentration

The effect of different Cu(II) concentrations was determined after experimental studies for a range of metal concentrations. A definite mass of Ca–Al–Zn LDH adsorbent (0.25 g/l) was added to a series of 100 ml of copper solutions with the different initial concentrations of 10, 15, 20, 25, 30, 35, 40, 45, 50, and 55 mg/l at pH 6.0 and were shaken at 160 rpm for contact time 120 min to reach the equilibrium. The Cu(II) removal shown in Fig. 10 indicates that calcined and uncalcined Ca–Al–Zn LDHs apparently removed a considerable amount of copper ions from the aqueous solutions. The adsorption capacity increased to 14 and 20 mg/g for calcined and uncalcined Ca–Al–Zn LDHs, respectively, and saturated beyond a certain concentration. Saturation resulted when no more metal ions could be adsorbed on the surface of calcined and uncalcined Ca–Al–Zn LDHs where the adsorption occurred. The experimental studies also showed that the high capacity for Cu(II) removal could be obtained over a relatively short period of time up to 120 min. The removal with initial Cu(II) concentrations means that the removal amounts were linearly proportional to the initial metal concentrations. However, the complete removal of copper ions was observed at 10, 15, 20, 25, 30, and 35 mg/l and 10, 15, 20, 25, 30, 35, 40, 45, and 50 mg/l from the initial concentrations (55 mg/l) for uncalcined and calcined Ca–Al–Zn LDHs adsorbents, respectively.

3.3. Effect of contact time

Fig. 11 shows that the effect of contact time on the adsorption capacity and percentage removal of Cu(II) 55 mg/l initial concentration onto 0.25 g/l calcined and uncalcined Ca–Al–Zn LDHs at pH 6.0, shaking rate 160 rpm and 25°C. It can be seen that the adsorption rate was considerably fast within the first 30 min (3.3 and 8.7 mg of Cu(II) adsorbed per gram of uncalcined and calcined Ca–Al–Zn LDHs, respectively), then gradually slowed down, and thereafter, the adsorption equilibrium was reached at 120 min (15.4 and 20.5 mg of Cu(II) adsorbed per

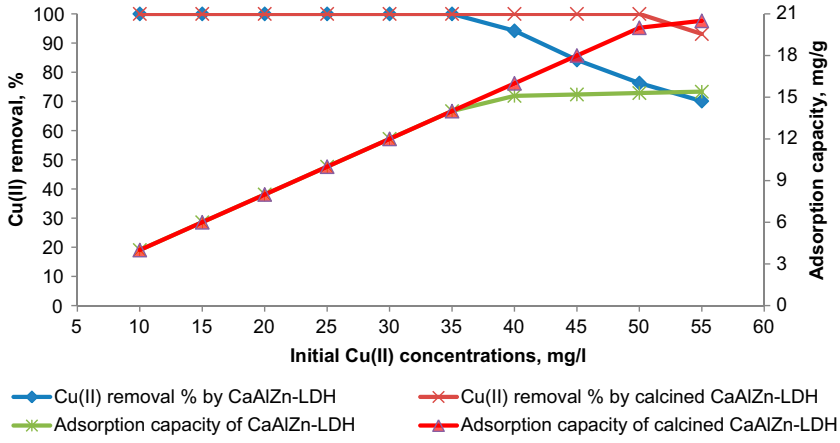

Fig. 10. Effect of initial Cu(II) concentrations on the removal percentages and adsorption capacities for calcined and uncalcined Ca–Al–Zn LDHs.

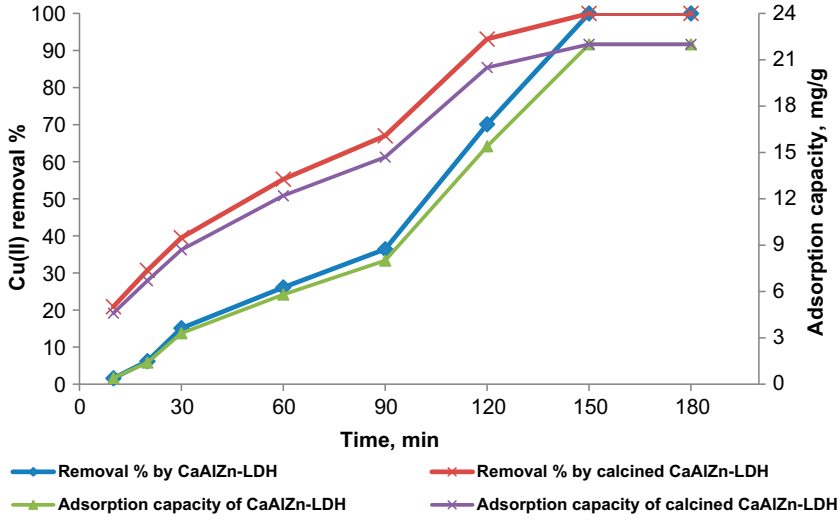

Fig. 11. Effect of contact time on the percentages of Cu(II) removal and adsorption capacities for calcined and uncalcined Ca–Al–Zn LDHs.

gram of uncalcined and calcined Ca–Al–Zn LDHs, respectively). The fast rate of Cu(II) removal in the beginning may be attributed to the rapid diffusion of Cu(II) from the solution to the external surfaces of calcined and uncalcined Ca–Al–Zn LDHs. On the other hand, the slow adsorption process is attributed to the longer diffusion range of Cu(II) into the inner-sphere of Ca–Al–Zn LDH or the ion exchange in the inner surface of calcined and uncalcined Ca–Al–Zn LDHs. Such slow diffusion will lead to a slow increase in the adsorption curve at later stages [40]. Moreover, the initial rapid adsorption may be because of an increased number of available sites at the initial stage.

3.4. Effect of initial solution pH

The effect of starting solution pH on the Cu(II) removal percentage from aqueous solutions with an initial concentrations of 55 mg/l using 0.25 g/l calcined and uncalcined Ca–Al–Zn LDHs after 120 min are shown in Fig. 12. The effect of starting solution pH on the Cu(II) removal percentage can be divided into three regions. For calcined and uncalcined Ca–Al–Zn LDHs masses of 0.25 g/l, the removal percentages of Cu(II) (55 mg/l) are 32.9 and 4.3%, respectively, at pH 2 within the pH range 2–4 (region I), while in region II (pH 4–6), the Cu(II) adsorption increases with increasing pH value, and reaches 93.1

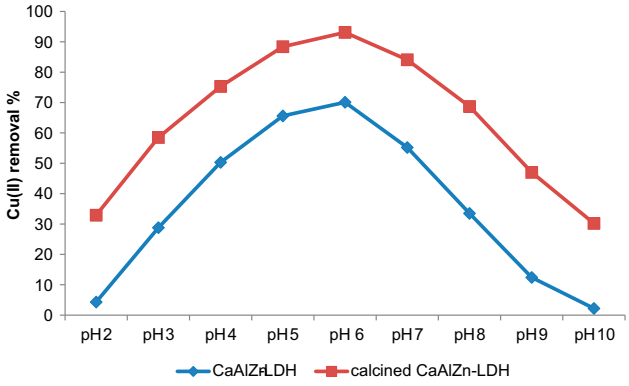

Fig. 12. Effect of initial solution pH on the removal percentages of 55.0 mg/l Cu(II) concentration at 0.25 g/l of adsorbent mass for calcined and uncalcined Ca–Al–Zn LDHs.

and 70.1% for calcined and uncalcined Ca–Al–Zn LDHs, respectively, at pH 6. Next, the removal percentage decreases with increasing pH (region III) and appears to reach a minimum value of 30.2% and 2.2% for calcined and uncalcined Ca–Al–Zn LDHs, respectively, at pH 10. The lower adsorption at the higher pH range may be due to the increasing competitive effect of OH-adsorption on LDH [41].

Furthermore, the increase of Cu(II) adsorption on Ca–Al–Zn LDH with increasing pH may be attributed to the surface properties of Ca–Al–Zn LDH in terms of surface charge and dissociation of functional groups. Also, the LDH surface contains a large number of binding sites and may become positively charged at low pH due to the protonation reaction on its surface. At high pH values, the LDH surface becomes negatively charged due to the deprotonation process. Consequently, the electrostatic repulsion decreases with raising pH because of the reduction of positive charge density on the adsorption edges, which enhances the adsorption of the positively charged ions through electrostatic force of attraction [41].

3.5. Effect of Ca–Al–Zn LDH mass

Different amounts of calcined and uncalcined Ca–Al–Zn LDHs (0.10, 0.15, 0.20, 0.25, 0.30, 0.35, 0.40, 0.45, 0.50, and 0.55 g/l) were added to a series of 100 ml of copper ions solutions with initial concentration of 55 mg/l at pH 6.0, were shaken at 160 rpm for contact time 120 min to reach the equilibrium. Then, the aqueous samples were filtered, and the residual Cu(II) concentrations were analyzed.

The effect of the LDH adsorbent masses on the adsorption of Cu(II) in 55 mg/l solutions are shown in Fig. 13. For these experiments, the metal solutions containing the appropriate adsorbent mass were loaded in 100 ml snap-seal polyethylene bottles, which were then shaked at 160 rpm for 120 min. The mixture in each bottle was then centrifuged immediately, and the Cu(II) concentrations in the supernatant solutions were determined by spectrophotometer. As expected, the percentage of Cu(II) removed first increases sharply with an increase in LDH mass, at fixed initial adsorbate concentrations, and then levels off at an

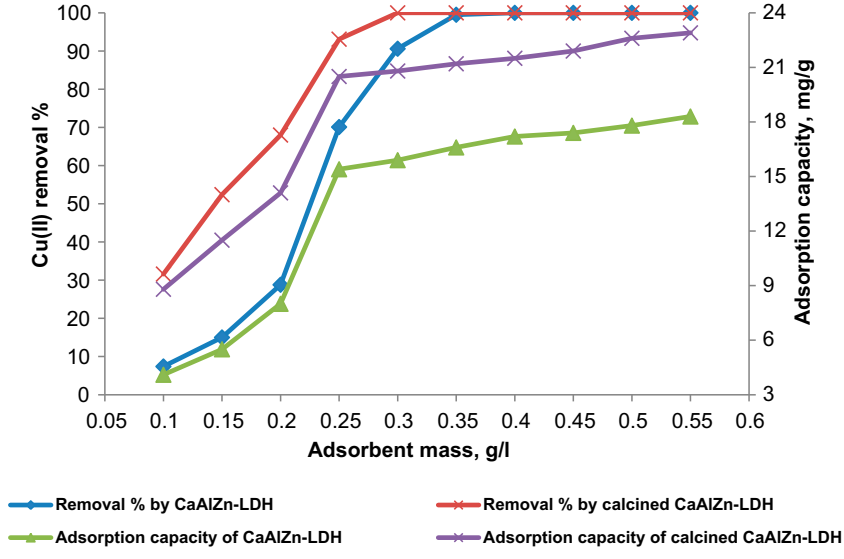

Fig. 13. The adsorbent masses as a function of Cu(II) removal percentages and adsorption capacities of calcined and uncalcined Ca–Al–Zn LDHs.

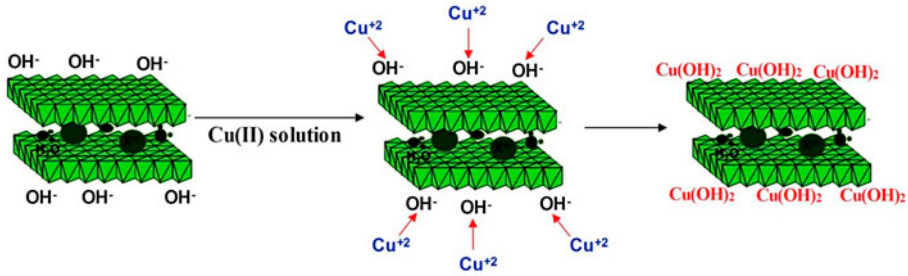

Scheme 1. Schematic diagram of copper removal using LDHs.

adsorbent mass above 0.30 g/l for calcined Ca–Al–Zn LDH and above 0.35 g/l for uncalcined Ca–Al–Zn LDH. On the other hand, the adsorption capacities of the materials decrease with increasing LDH masses [4].

Furthermore, even for the first LDH mass, when the adsorbent mass was 0.10 g/l, the adsorption capacities of calcined and uncalcined Ca–Al–Zn LDHs were 17.4 and 4.1 mg/g and reach a maximum values at adsorbent mass 0.25 g/l where the adsorption capacities are 20.5 and 15.4 mg/g, respectively.

3.6. Adsorption mechanism

In the studies of the adsorption of heavy metals from wastewater, LDHs could adsorb metal cations from aqueous solution in spite of positive layer charge [42,43]. Park et al. reported that a major reaction could be surface-induced precipitation that occurs due to localized high pH values and the released carbonate ions available to metal cations [44]. Positive layer charge attracts hydroxide ions around the surfaces of LDH crystals in aqueous solution to induce formation of metal hydroxides as shown in Scheme 1. Meanwhile, charge-compensating carbonate ion attached on the surface and edge could also contact with metal cations to form insoluble metal carbonates. There is also another possibility to adsorb metal cations via diodachy, as suggested by Komarneni et al. [45]. The reaction of Cu(II) solution with Ca–Al–Zn LDH gives rise to considerable precipitation of copper hydroxide species on the external surfaces of LDH crystals, which could protect LDH framework from being attacked by further reaction. Eventually, rapid equilibrium could be established between Cu^{2+} in solution and copper hydroxide precipitated on the LDH surfaces [44].

4. Conclusion

A novel Ca–Al–Zn LDH intercalated with carbonate $(CO_3)^{2-}$ as interlayer anion was successfully synthesized by co-precipitation method, and its structure was well characterized by XRD, FT-IR, N2 adsorption–desorption isotherm, and SEM. The removal of copper ions was shown to be dependent on pH, contact time, adsorbent mass, and initial adsorbate concentration. This study shows that Ca–Al–Zn LDH is a suitable adsorbent for the removal of Cu(II) from aqueous solutions and its calcined product (calcined Ca–Al–Zn LDH) which is obtained by heating at 450°C for 4.0 h has higher potential application in Cu (II) ions removal field.

References

[1] F. Cavani, F. Trifirò, A. Vaccari, Hydrotalcite-type anionic clays: Preparation, properties and applications, Catal. Today 11 (1991) 173–301.
[2] J. Das, B.S. Patra, N. Baliarsingh, K.M. Parida, Adsorption of phosphate by layered double hydroxides in aqueous solutions, Appl. Clay Sci. 32 (2006) 252–260.
[3] L.P. Patricio Cardoso, J.B. Valim, Competition between three organic anions during regeneration process of calcined LDH, J. Phys. Chem. Solids 65 (2004) 481–485.
[4] D.P. Das, J. Das, K.M. Parida, Physicochemical characterization and adsorption behavior of calcined Zn/Al hydrotalcite-like compound (HTlc) towards removal of fluoride from aqueous solution, J. Colloid Interface Sci. 261 (2003) 213–220.
[5] T. Sato, T. Wakabayashi, M. Shimada, Adsorption of various anions by magnesium aluminum oxide of ($Mg_{0.7}Al_{0.3}O_{1.15}$), Ind. Eng. Chem. Prod. Res. Dev. 25 (1986) 89–92.
[6] K. Chibwe, W. Jones, Synthesis of polyoxometalate pillared layered double hydroxides via calcined precursors, Chem. Mater. 1 (1989) 489–490.
[7] V.R.L. Constantino, T.J. Pinnavaia, Basic properties of $Mg^{2+}_{1-x}Al^{3+}_{x}$ layered double hydroxides intercalated by carbonate, hydroxide, chloride, and sulfate anions, Inorg. Chem. 34 (1995) 883–892.
[8] R.L. Goswamee, P. Sengupta, K.G. Bhattacharyya, D.K. Dutta, Adsorption of Cr(VI) in layered double hydroxides, Appl. Clay Sci. 13 (1998) 21–34.
[9] S. Tezuka, R. Chitrakar, K. Sakane, A. Sonoda, K. Ooi, T. Tomida, The synthesis and phosphate adsorptive properties of Mg(II)–Mn(III) layered double hydroxides and their heat-treated materials, Bull. Chem. Soc. Jpn. 77 (2004) 2101–2107.

[10] J. Das, B.S. Sairam Patra, N. Baliarsingh, K.M. Parida, Calcined Mg–Fe–CO_3 LDH as an adsorbent for the removal of selenite, J. Colloid Interface Sci. 316 (2007) 216–223.
[11] F. Bruna, R. Celis, I. Pavlovic, C. Barriga, J. Cornejo, M.A. Ulibarri, Layered double hydroxides as adsorbents and carriers of the herbicide (4-chloro-2-methylphenoxy)acetic acid (MCPA): Systems Mg–Al, Mg–Fe and Mg–Al–Fe, J. Hazard. Mater. 168 (2009) 1476–1481.
[12] J. Das, D. Das, G.P. Dash, D. Das, K. Parida, Studies on Mg/Fe hydrotalcite-like-compound (HTlc): Removal of Chromium(VI) from aqueous solution, Int. J. Environ. Stud. 61 (2004) 605–616.
[13] A.A. Bakr, M.M. Kamel, A. Hamdy, Z.M. Khaled, M.A. Abbas, Reverse osmosis pretreatment: Removal of iron in groundwater desalination plant in Shupramant-Giza—A case study, Curr. World Environ. 7 (2012) 23–32.
[14] A.A. Bakr, W.A. Makled, New pretreatment media filtration for SWRO membranes of desalination plants, Desalin. Water Treat. (2014) 1–13.
[15] A.A. Bakr, M.S. Mostafa, Gh Eshaq, M.M. Kamel, Kinetics of uptake of Fe(II) from aqueous solutions by Co/Mo layered double hydroxide (Part 2), Desalin. Water Treat. (2014) 1–8.
[16] M.S. Mostafa, A.A. Bakr, Gh Eshaq, M.M. Kamel, Novel Co/Mo layered double hydroxide: synthesis and uptake of Fe(II) from aqueous solutions (Part 1), Desalin. Water Treat. (2014) 1–9.
[17] N.N. Das, J. Konar, M.K. Mohanta, S.C. Srivastava, Adsorption of Cr(VI) and Se(IV) from their aqueous solutions onto Zr^{4+}-substituted ZnAl/MgAl-layered double hydroxides: Effect of Zr^{4+} substitution in the layer, J. Colloid Interface Sci. 270 (2004) 1–8.
[18] M. Olivares, F.S.H. Pizarro, H. Speisky, B. Lönnerdal, Copper in infant nutrition: Safety of World Health Organization provisional guideline value for copper content of drinking water, J. Pediatr. Gastroenterol. Nutr. 26 (1998) 251–257.
[19] A.A. Bakr, Y.M. Moustafa, M.M.H. Khalil, M.M. Yehia, E.A. Motawea, Magnetic nano-composite beads: Synthesis and uptake of Cu(II) ions from aqueous solutions, Can. J. Chem. 93(3) (2015) 289–296.
[20] J. Tseng, C. Chang, Y. Chen, C. Chang, P. Chiang, Synthesis of micro-size magnetic polymer adsorbent and its application for the removal of Cu(II) ion, Colloids Surf., A 295 (2007) 209–216.
[21] M.A. Gonzلlez, I. Pavlovic, C. Barriga, Cu(II), Pb(II) and Cd(II) sorption on different layered double hydroxides. A kinetic and thermodynamic study and competing factors, Chem. Eng. J. 269 (2015) 221–228.
[22] J.S. Valente, E. Lopez-Salinas, M.S. Cantu, F. Hernandez-Beltran, US Patent 0189481 A1 (2006).
[23] S.V. Jaime, T. Francisco, P. Julia, G.H.C. Jose, G. Ricardo, Adsorption and photocatalytic degradation of phenol and 2,4-dichlorophenoxiacetic acid by Mg–Zn–Al layered double hydroxides, Appl. Catal. B: Environ. 90 (2009) 330–338.
[24] A. Legrouri, M. Lakraimi, A. Barroug, A.D. De Roy, J.P. Besse, Removal of the herbicide 2,4-dichlorophenoxyacetate from water to zinc–aluminium–chloride layered double hydroxides, Water Res. 39 (2005) 3441–3448.
[25] R.R. Delgado, C.P.D. Pauli, C.B. Carrasco, M.J. Avena, Influence of M^{II}/M^{III} ratio in surface-charging behavior of Zn-Al layered double hydroxides, Appl. Clay Sci. 40 (2008) 23–27.
[26] R. Vicente, S. Kannan, Layered double hydroxides with the hydrotalcite-type structure containing Cu^{2+}, Ni^{2+} and Al^{3+}, J. Mater. Chem. 10 (2000) 489–495.
[27] W. Yang, Y. Kim, P.K.T. Liu, M. Sahimi, T.T. Tsotsis, A study by in situ techniques of the thermal evolution of the structure of a Mg–Al–CO_3 layered double hydroxide, Chem. Eng. Sci. 57 (2002) 2945–2953.
[28] M. Sato, H. Kuwabara, S. Sato, Characterization of anion exchanged hydrotalcite and determination of the site of exchanged SO_4 group, Clay Sci. 8 (1992) 309–317.
[29] C.O. Oriakhi, I.V. Farr, M.M. Lerner, Incorporation of poly(acrylic acid), poly(vinylsulfonate) and poly (styrenesulfonate) within layered double hydroxides, J. Mater. Chem. 6 (1996) 103–107.
[30] T. Hibino, Y. Yamashita, K. Kosuge, A. Tsunashima, Decarbonation behavior of Mg-Al-CO_3 hydrotalcite-like compounds during heat treatment, Clays Clay Miner. 43 (1995) 427–432.
[31] K. Nakanishi, Infrared Absorption Spectroscopy-Practical, Nankodo Company Ltd., Tokyo, 1962 pp. 54–55.
[32] Y. Zheng, N. Li, W. Zhang, Preparation of nanostructured microspheres of Zn–Mg–Al layered double hydroxides with high adsorption property, Colloids Surf., A 415 (2012) 195–201.
[33] M. Lakraimi, A. Legrouri, A. Barroug, A.D. De Roy, J.P. Pierre Besse, Preparation of a new stable hybrid material by chloride–2,4-dichlorophenoxyacetate ion exchange into the zinc–aluminium–chloride layered double hydroxide, J. Mater. Chem. 10 (2000) 1007–1011.
[34] K.S.W. Sing, D.H. Everett, R.A.W. Haul, L. Moscow, R.A. Pierotti, J. Rouqerd, T. Siemieniewska, Reporting physisorption data for gas/solid systems with Special Reference to the Determination of Surface Area and Porosity, Pure Appl. Chem. 57 (1985) 603–619.
[35] A. Lecloux, J.P. Pirard, The importance of standard isotherms in the analysis of adsorption isotherms for determining the porous texture of solids, J. Colloid Interface Sci. 70 (1979) 265–281.
[36] S. Brunauer, P.H. Emmett, E. Teller, Adsorption of gases in multimolecular layers, J. Am. Chem. Soc. 60 (1938) 309–319.
[37] E. Barrett, L.G. Joyner, P.P. Halenda, The determination of pore volume and area distributions in porous substances. I. Computations from nitrogen isotherms, J. Am. Chem. Soc. 73 (1951) 373–380.
[38] M.H. Al-Qunaibit, W.K. Mekhemer, A.A. Zaghloul, The adsorption of Cu(II) ions on bentonite—A kinetic study, J. Colloid Interface Sci. 283 (2005) 316–321.
[39] E. Barrett, L.G. Joyner, P.P. Halenda, The determination of pore volume and area distributions in porous substances. I. computations from nitrogen isotherms, J. Am. Chem. Soc. 73 (1951) 373–380.
[40] H. Song, F. Jiao, X. Jiang, J. Yu, X. Chen, S. Du, Removal of vanadate anion by calcined Mg/Al-CO_3 layered double hydroxide in aqueous solution, Trans. Nonferrous Met. Soc. China 23 (2013) 3337–3345.

[41] D. Zhao, G. Sheng, J. Hu, C. Chen, X. Wang, The adsorption of Pb(II) on Mg_2Al layered double hydroxide, Chem. Eng. J. 171 (2011) 167–174.
[42] T. Kameda, S. Saito, Y. Umetsu, Mg-Al layered double hydroxide intercalated with ethylene-diaminetetraacetate anion: Synthesis and application to the uptake of heavy metal ions from an aqueous solution, Sep. Purif. Technol. 47 (2005) 20–26.
[43] M.R. Pérez, I. Pavlovic, C. Barriga, J. Cornejo, M.C. Hermosín, M.A. Ulibarri, Uptake of Cu^{2+}, Cd^{2+} and Pb^{2+} on Zn–Al layered double hydroxide intercalated with edta, Appl. Clay Sci. 32 (2006) 245–251.
[44] M. Park, C.L. Choi, Y.J. Seo, S.K. Yeo, J. Choi, S. Komarneni, J.H. Lee, Reactions of Cu^{2+} and Pb^{2+} with Mg/Al layered double hydroxide, Appl. Clay Sci. 37 (2007) 143–148.
[45] S. Komarneni, N. Kozai, R. Roy, Novel function for anionic clays: Selective transition metal cation uptake by diadochy, J. Mater. Chem. 8 (1998) 1329–1331.